

A macrocyclic receptor containing two viologen species connected by conjugated terphenyl groups

Article

Supplemental Material

Chen, L., Lim, K. J. C., Babra, T. S., Taylor, J. O., Pižl, M., Evans, R., Chippindale, A. M. ORCID: <https://orcid.org/0000-0002-5918-8701>, Hartl, F. ORCID: <https://orcid.org/0000-0002-7013-5360>, Colquhoun, H. M. and Greenland, B. W. (2018) A macrocyclic receptor containing two viologen species connected by conjugated terphenyl groups. *Organic & Biomolecular Chemistry*, 16 (27). pp. 5006-5015. ISSN 1477-0520 doi: 10.1039/c8ob00919h Available at <https://centaur.reading.ac.uk/78400/>

It is advisable to refer to the publisher's version if you intend to cite from the work. See [Guidance on citing](#).

Published version at: <http://dx.doi.org/10.1039/c8ob00919h>

To link to this article DOI: <http://dx.doi.org/10.1039/c8ob00919h>

Publisher: Royal Society of Chemistry

www.reading.ac.uk/centaur

CentAUR

Central Archive at the University of Reading

Reading's research outputs online

Supporting Information

A macrocyclic receptor containing two viologen species connected by conjugated terphenyl groups

Long Chen,^a Kate J. C. Lim,^a Tahkur S. Babra,^a James O. Taylor,^a Martin Pižl,^{b,c} Robert Evans,^d Ann M. Chippindale,^a František Hartl,^a Howard M. Colquhoun^{*a} and Barnaby W. Greenland^{*a,e}

^aDepartment of Chemistry, University of Reading, Whiteknights, Reading, RG6 6AD, UK; email: h.m.colquhoun@reading.ac.uk

^b J. Heyrovský Institute of Physical Chemistry, Academy of Sciences of the Czech Republic, Dolejškova 3, CZ-182 23 Prague, Czech Republic

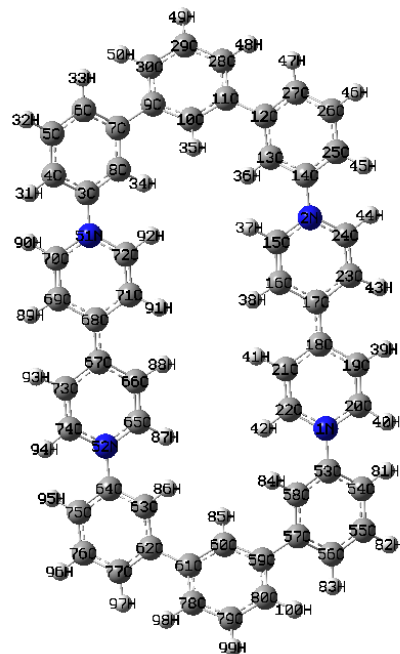
^c Department of Inorganic Chemistry, University of Chemistry and Technology, Prague, Technická 5, CZ-166 28 Prague, Czech Republic

^d Aston University Institute of Materials Research, School of Engineering and Applied Science, Birmingham, B4 7ET, UK.

^e Department of Chemistry, School of Life Sciences, University of Sussex, Falmer, BN1 9QJ, UK; email b.w.greenland@sussex.ac.uk

Contents	Page
Table S1 Atom numbering and comparison of structural data of 4⁴⁺ from solid state analysis and DFT calculations.....	S2
Table S2 Selected DFT calculated bond lengths and angles for 4⁴⁺ , 4^{2(•+)} and 4	S3
Table S3. TD-DFT (PBE0/PCM-MeCN) calculated low-lying transitions of triplet 4^{2(•+)} with oscillator strength higher than 0.005).....	S5
Figure S1 Molecular orbitals of 4⁴⁺ involved in the calculated transition at 339 nm	S6
Figure S2 Molecular orbitals of 4^{2(•+)} involved in the calculated transition at 584 nm.....	S6
Figure S3 Molecular orbitals of 4 involved in the calculated transition at 453 nm.....	S7
Figure S4 Calculated electronic absorption spectra for 4^{2(•+)} with vertical excitations.....	S7
Figure S5 Calculated α-spinorbitals of 4^{2(•+)} involved in UV-vis electronic transitions.....	S8
Figure S6 Calculated b-spinorbitals of 4^{2(•+)} involved in UV-vis electronic transitions.....	S9
Figure S7 DOSY NMR data.....	S10
Figure S8 ¹ H and ¹³ C NMR spectra for 4⁴⁺	S11
Figure S9 ¹ H and ¹³ C NMR spectra for 10	S12

Table S1. A comparison of selected experimental and *in vacuo* DFT calculated bond lengths (Å) and angles (°) for **4⁴⁺**.



Macrocyclic **4⁴⁺** with atoms numbered.

Bond	Exp.	Calc. (<i>in vacuo</i>)	Angle	Exp.	Calc. (<i>in vacuo</i>)
N51-C3	1.451	1.447	N51-C3-C8	118.3	117.7
N52-C64	1.450	1.447	C3-N51-C72	117.8	118.5
N1-C53	1.451	1.447	C71-C68-C67	120.5	117.9
N2-C14	1.450	1.447	C68-C67-C66	120.6	117.9
N1-C22	1.353	1.349	C65-N52-C64	119.8	118.5
C22-C21	1.375	1.374	N52-C64-C63	117.8	117.7
C21-C18	1.368	1.398	N2-C14-C13	117.8	117.7
C18-C17	1.470	1.484	C14-N2-C15	119.8	118.5
C17-C16	1.397	1.398	C16-C17-C18	120.6	117.9
C16-C15	1.355	1.374	C17-C18-C21	120.5	117.9
C15-N2	1.352	1.349	C22-N1-C53	117.8	118.5
N52-C65	1.352	1.349	N1-C53-C58	118.3	117.7
C65-C66	1.355	1.374			
C66-C67	1.397	1.398			
C67-C68	1.470	1.484			
C68-C71	1.368	1.398			
C71-C72	1.375	1.374			
C72-N51	1.353	1.349			

Table S2. Comparison of selected DFT calculated (polarizable continuum model, PCM-MeCN) bond lengths (Å) and angles (°) for **4⁴⁺**, **4^{2(•+)}** and **4** (for atom numbering see Table S1).

Note the strong variation in the C-N and C-C bond lengths in the heterocycle rings (**red entries**) for each of the sequential oxidation states of the macrocycle (**4⁴⁺**, **4^{2(•+)}** and **4**). In contrast, note the relative invariance with oxidation state of the bond lengths calculated in the polyaromatic spacer units (**purple entries**). The C-N bonds between the heterocycle rings and polyaromatic spacer units (**green entries**) also become shorter upon the reduction, which is ascribed to a better π-overlap between C(p) and N(p) orbitals due increasing planarity of the viologen units (Figure 6 in the main text).

Bond	Bond Length (Å)		
	4⁴⁺	4^{2(•+)}	4
N51-C3	1.442	1.424	1.403
N52-C64	1.442	1.425	1.403
N1-C53	1.442	1.424	1.403
N2-C14	1.442	1.425	1.403
N1-C22	1.350	1.370	1.391
C22-C21	1.373	1.358	1.346
C21-C18	1.395	1.422	1.448
C18-C17	1.473	1.423	1.381
C17-C16	1.395	1.422	1.448
C16-C15	1.373	1.358	1.346
C15-N2	1.349	1.370	1.390
N52-C65	1.349	1.370	1.390
C65-C66	1.373	1.358	1.346
C66-C67	1.395	1.422	1.448
C67-C68	1.473	1.423	1.381
C68-C71	1.395	1.422	1.448
C71-C72	1.373	1.358	1.346
C72-N51	1.350	1.370	1.391
C3-C8	1.386	1.390	1.397
C8-C7	1.395	1.395	1.395
C7-C9	1.476	1.476	1.477
C9-C10	1.395	1.394	1.395
C10-C11	1.394	1.394	1.395
C11-C12	1.476	1.476	1.477
C12-C13	1.395	1.395	1.395
C13-C14	1.386	1.389	1.397
C53-C58	1.386	1.390	1.397
C58-C57	1.395	1.395	1.395
C57-C59	1.476	1.476	1.477
C59-C60	1.395	1.394	1.395
C60-C61	1.394	1.394	1.395

	Bond Angle (°)		
	4⁴⁺	4^{2(•+)}	4
N51-C3-C8	118.2	119.1	120.1
C3-N51-C72	119.2	120.4	121.4
C71-C68-C67	120.2	122.2	123.4
C68-C67-C66	120.1	122.2	123.4
C65-N52-C64	119.1	120.4	121.3
N52-C64-C63	118.3	119.1	120.0
N2-C14-C13	118.3	119.1	120.0
C14-N2-C15	119.1	120.4	121.3
C16-C17-C18	120.1	122.2	123.4
C17-C18-C21	120.1	122.2	123.4
C22-N1-C53	119.1	120.4	121.4
N1-C53-C58	118.2	119.1	120.1

C61-C62	1.476	1.476	1.477
C62-C63	1.395	1.395	1.395
C63-C64	1.386	1.389	1.397

|

Table S3. TD-DFT (PBE0/PCM-MeCN) calculated low-lying transitions of triplet **4²⁽⁺⁾** with oscillator strength higher than 0.005 (see Figure S7). Molecular spinorbitals involved in the electronic transitions are depicted in Figures S8 and S9.

Main component (%)	Transition energy [eV] (nm)	Oscillator strength
α -HOSO-1 → α -LUSO (68) α -HOSO → α -LUSO+1 (70)	2.04 (607)	Weak (~0)
α -HOSO-1 → α -LUSO+1 (68) α -HOSO → α -LUSO (68)	2.12 (584)	1.090
α -HOSO-1 → α -LUSO+2 (78) α -HOSO → α -LUSO+7 (35)	2.88 (431)	0.014
α -HOSO → α -LUSO+3 (71)	2.90 (428)	0.137
α -HOSO → α -LUSO+3 (40) β -HOSO-2 → β -LUSO (38) β -HOSO → β -LUSO+1 (49)	2.98 (416)	0.942
β -HOSO-1 → β -LUSO (62)	3.15 (394)	0.035
β -HOSO → β -LUSO+1 (44)	3.16 (392)	0.315
β -HOSO-1 → β -LUSO (64)	3.31 (374)	0.006
β -HOSO → β -LUSO+1 (65) β -HOSO-4 → β -LUSO+1 (45) β -HOSO-5 → β -LUSO (39)	3.33 (373)	0.439
β -HOSO-2 → β -LUSO (76) β -HOSO-5 → β -LUSO (41) β -HOSO-4 → β -LUSO+1 (40)	3.54 (351)	0.058
α -HOSO-1 → α -LUSO+8 (42) α -HOSO-1 → α -LUSO+13 (43) α -HOSO → α -LUSO+9 (48) α -HOSO → α -LUSO+12 (78)	3.60 (344)	0.029
α -HOSO-1 → α -LUSO+8 (57) α -HOSO → α -LUSO+9 (51)	3.61 (343)	0.020
α -HOSO-1 → α -LUSO+10 (78) α -HOSO → α -LUSO+11 (44) β -HOSO-3 → β -LUSO+1 (40)	3.62 (342)	0.013
β -HOSO-7 → β -LUSO (54) β -HOSO-6 → β -LUSO+1 (54)	3.83 (324)	0.13
Mixed	3.98 (312)	0.024
β -HOSO-12 → β -LUSO (59) β -HOSO-11 → β -LUSO+1 (59)	3.99 (311)	0.13
β -HOSO-13 → β -LUSO+1 (66) β -HOSO-14 → β -LUSO (67)	4.06 (305)	0.090

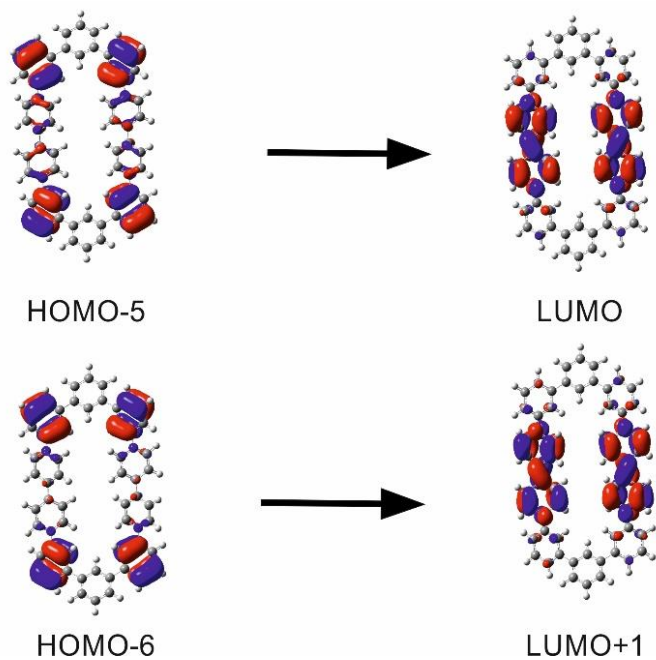


Figure S1. Molecular orbitals of $\mathbf{4}^{4+}$ involved in the calculated transition at 339 nm.

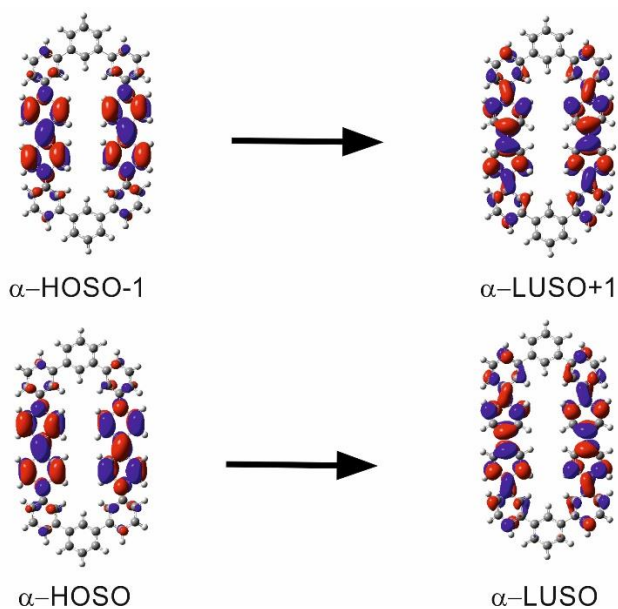


Figure S2. Molecular orbitals of $\mathbf{4}^{2(+)}$ involved in the calculated transition at 584 nm.

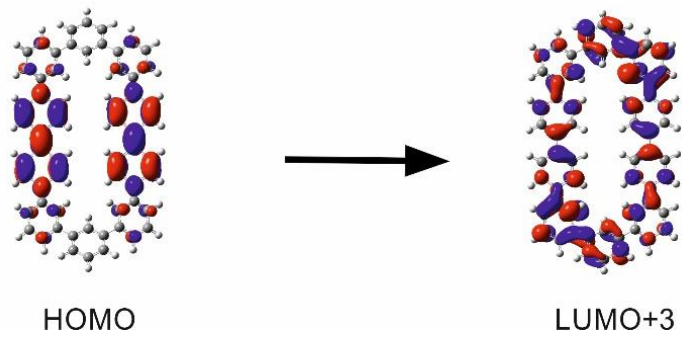


Figure S3. Molecular orbitals of **4** involved in the calculated transition at 453 nm.

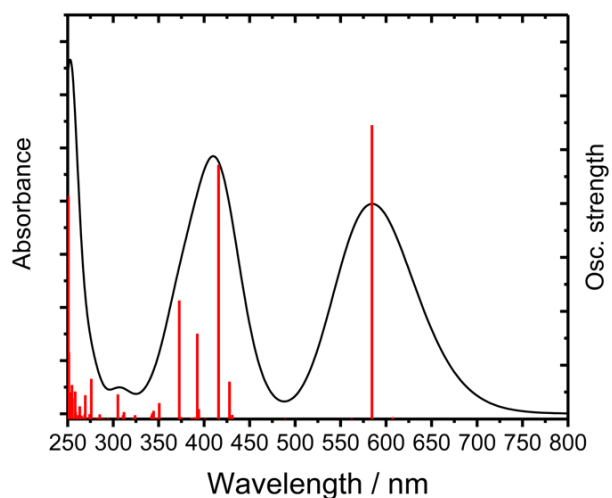


Figure S4. Calculated electronic absorption spectra for **4**²⁽⁺⁺⁾ with vertical excitations. (See Table S3 and Figures S5 and S6 for more details.)

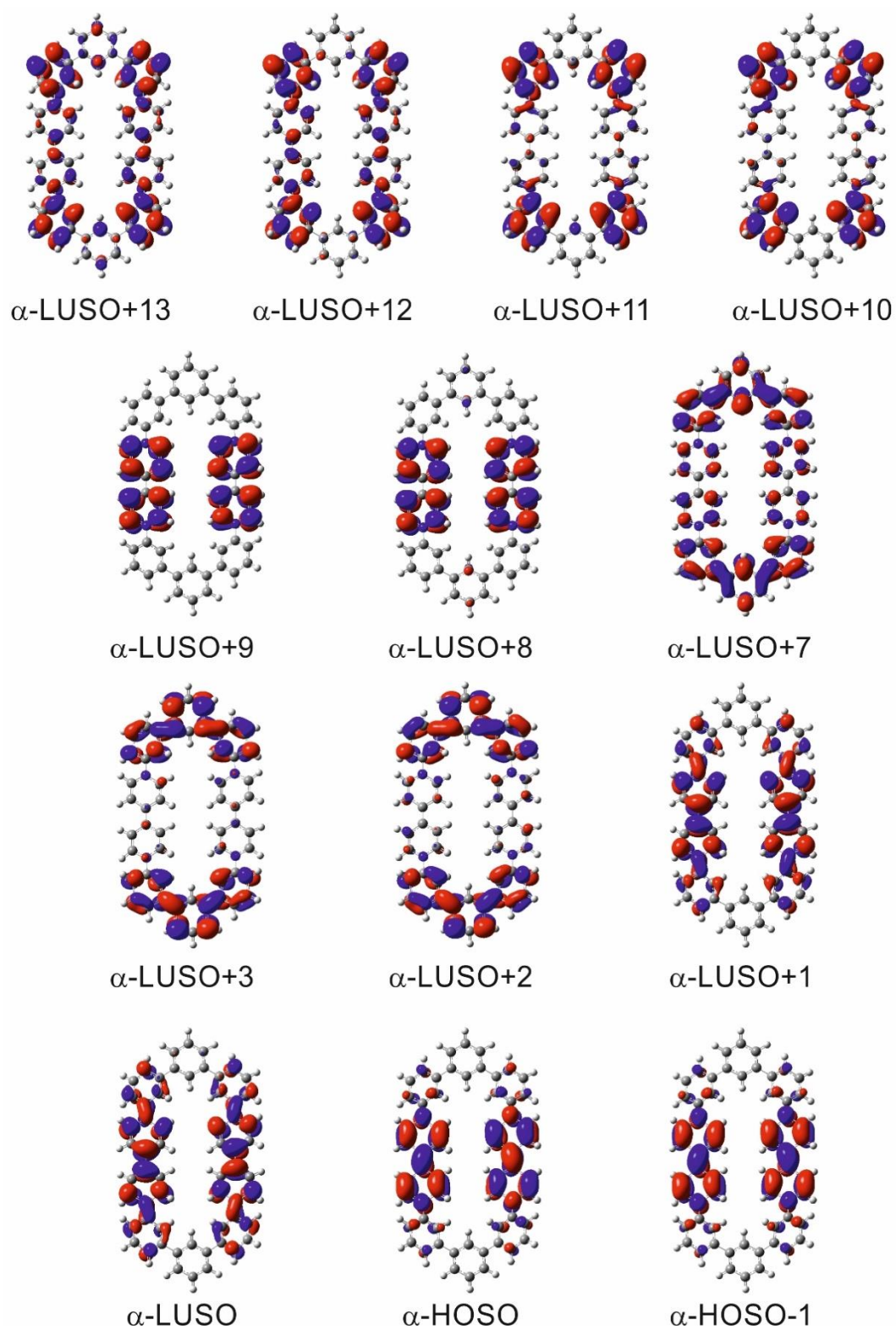


Figure S5. Calculated α -spinorbitals of $4^{2(\bullet+)}$ involved in the UV-vis electronic transitions (Table S3).

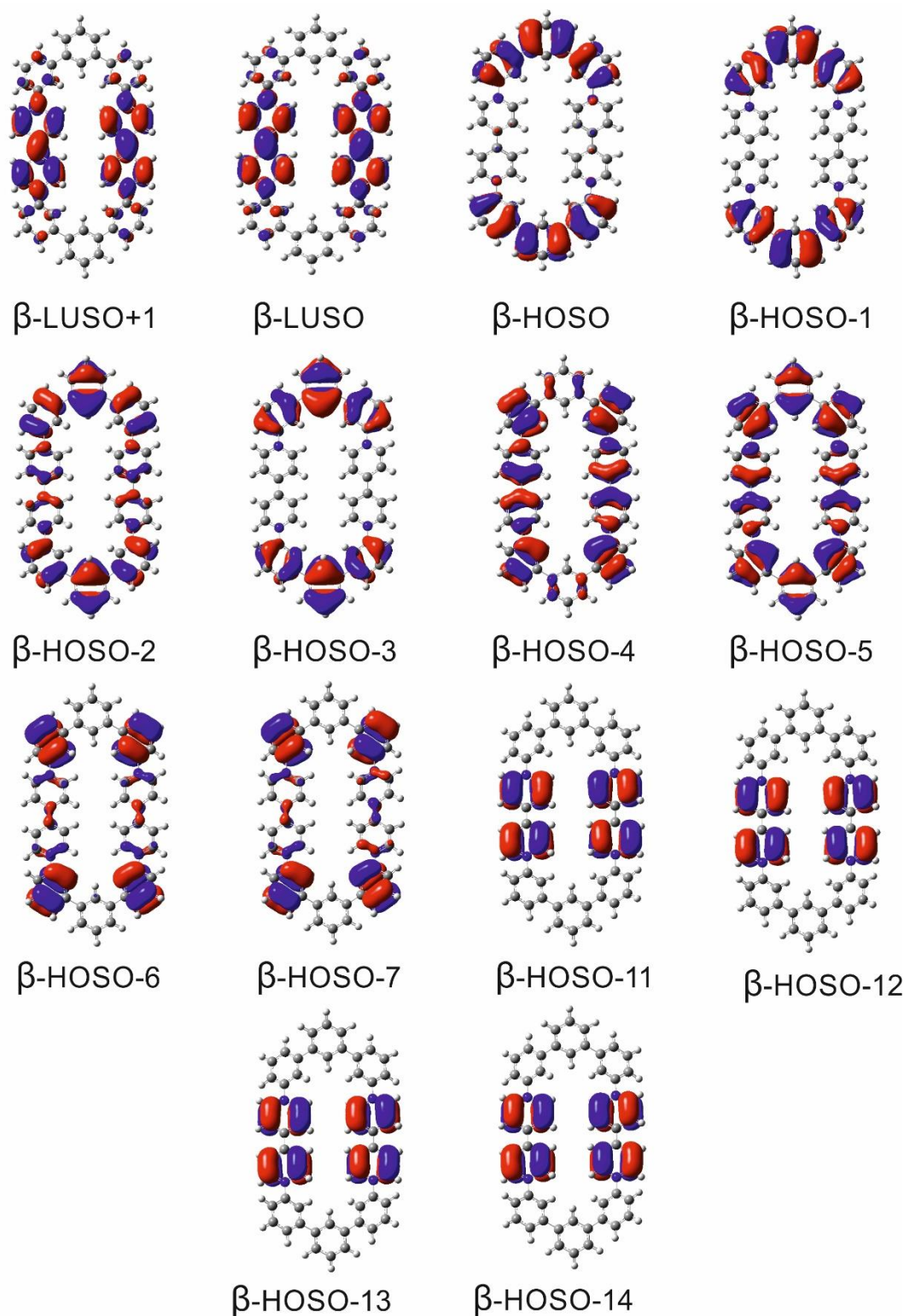


Figure S6. Calculated β -spin orbitals of $\mathbf{4}^{2(\bullet+)}$ involved in the UV-vis electronic transitions (Table S3).

DOSY ^1H NMR data

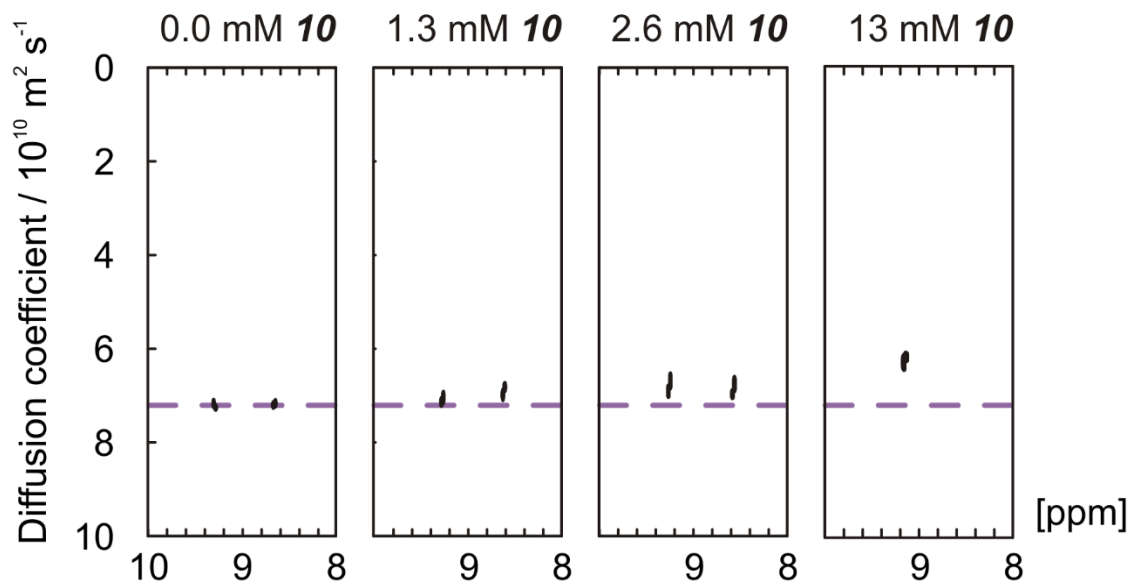


Figure S7. Four DOSY spectra (CD_3CN) corresponding to samples of 1.3 mM $\textbf{4}^{4+}$ and 0, 1.3, 2.6 and 13 mM **10** respectively (used to construct Figure 7 in the paper). Only the region between 8 and 10 ppm shown. In the sample containing 13 mM $\textbf{4}^{4+}$, peaks at ca. 8.5 ppm are not included in analysis due to overlap of signals from both species. Purple line indicates estimate for diffusion coefficient of $\textbf{4}^{4+}$ in the absence of any complexation.

^1H and ^{13}C NMR spectra of $\mathbf{4}^{4+}$

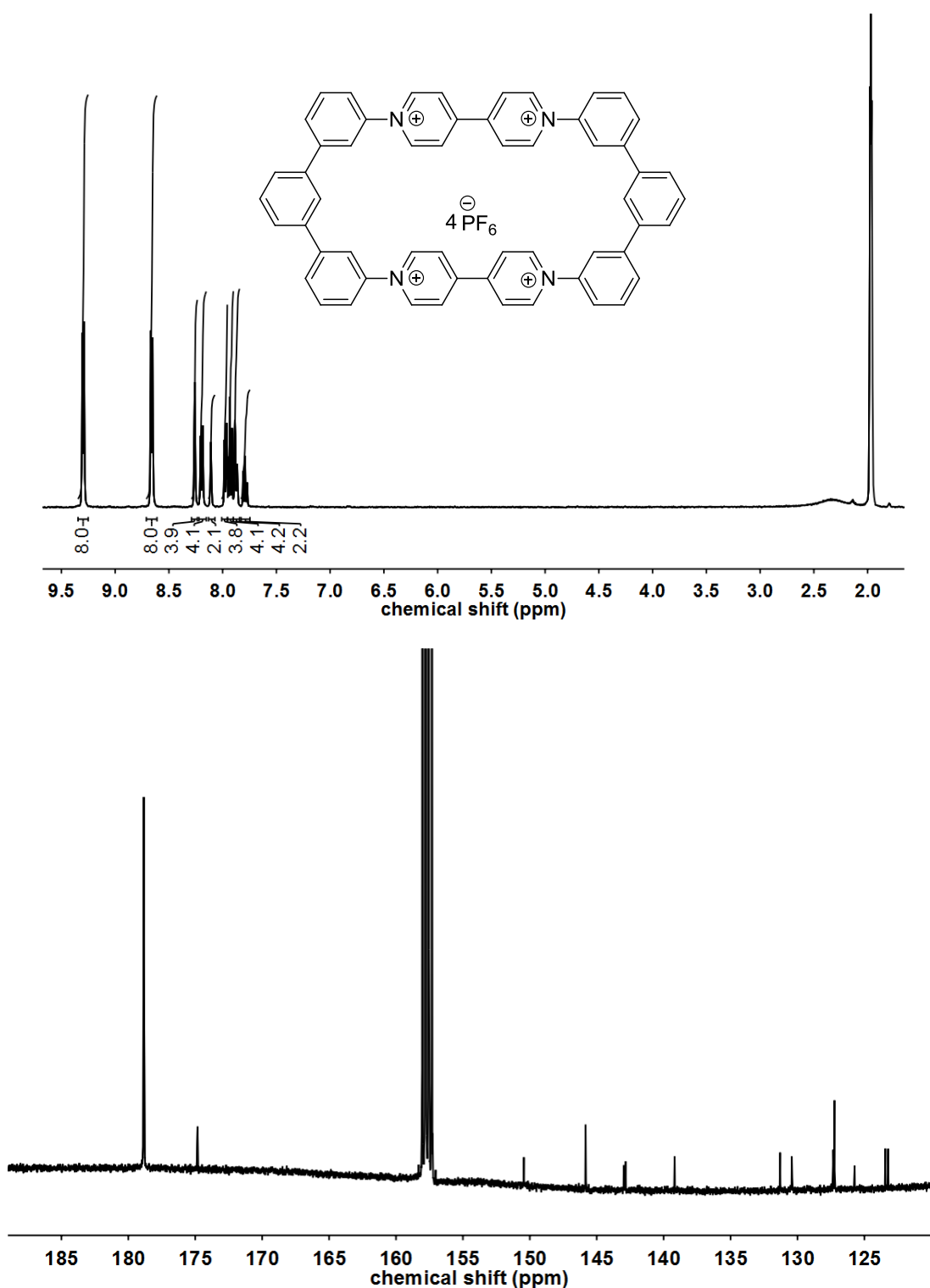


Figure S8. ^1H NMR $[(\text{CD}_3)_2\text{CO}, 400$ MHz] and ^{13}C NMR ($\text{CD}_3\text{CN}, 100$ MHz) spectra of $\mathbf{4}^{4+} \cdot 4(\text{PF}_6^-)$

¹H and ¹³C NMR spectra of **10**

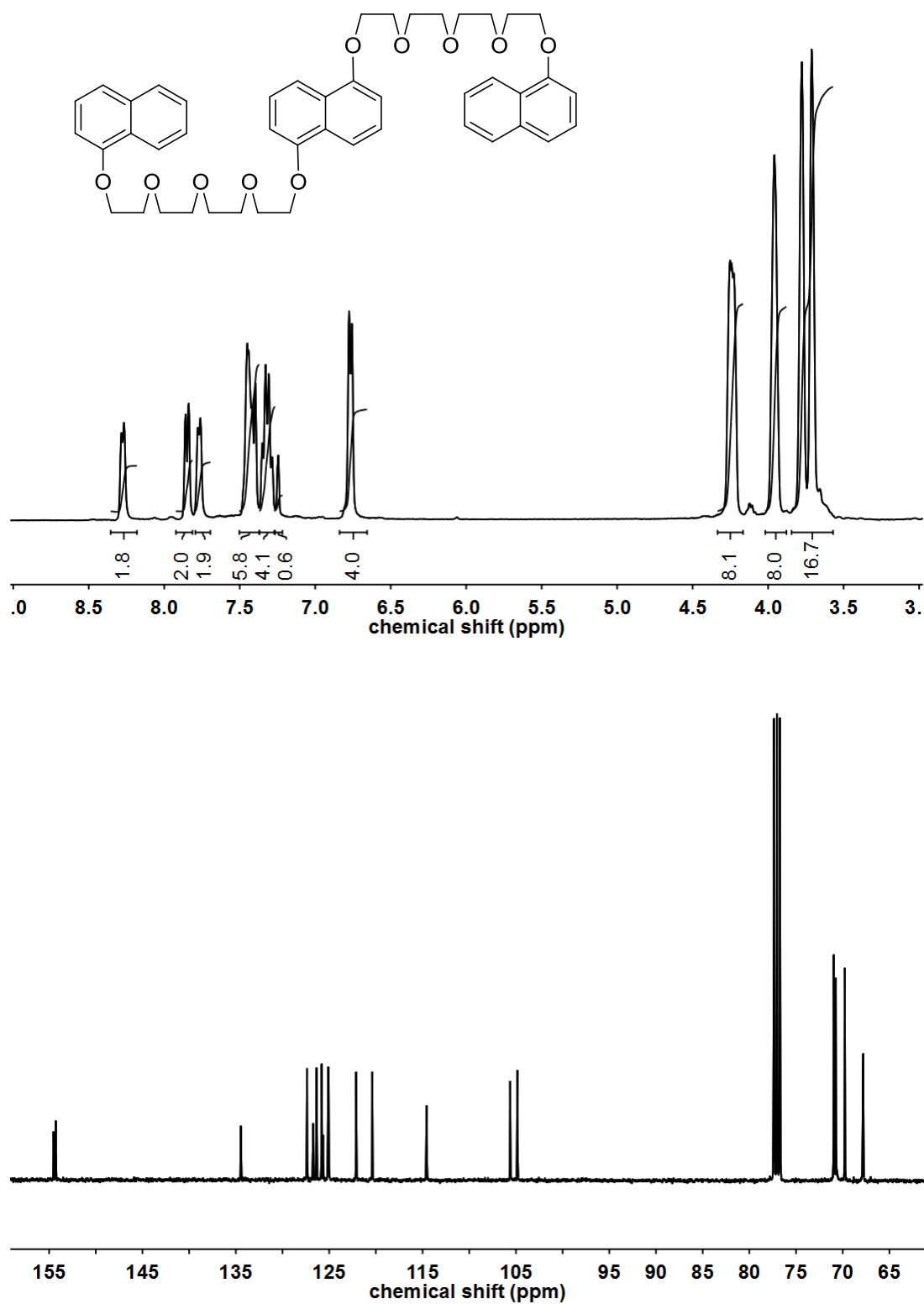


Figure S9. 400 MHz ¹H and 100 MHz ¹³C NMR spectra of **10** (CDCl_3)